Proc. 2015 IEEE International Conference on Intelligent Robots and Systems (IROS 2015)

Measuring Fingertip Forces from Camera Images for Random Finger Poses

Nutan Chen, Sebastian Urban, Justin Bayer, and Patrick van der Smagt

***Abstract*— Robust fingertip force detection from fingernail image is a critical strategy that can be applied in many areas. However, prior research fixed many variables that influence the finger color change. This paper analyzes the effect of the finger joint on the force detection in order to deal with the constrained finger position setting. A force estimator method is designed: a model to predict the fingertip force from finger joints measured from 2D cameras and 3 rectangular markers in cooperation with the fingernail images are trained. Then the error caused by the color changes of the joint bending can be avoided. This strategy is a significant step forward from a finger force estimator that requires tedious finger joint setting.**

The approach is evaluated experimentally. The result shows that it increases the accuracy over 10% for the force in conditions of the finger joint free movement. The estimator is used to demonstrate lifting and replacing objects with various weights.

I. Introduction

When studying the use of the human hand in grasping and manipulation [1], [2], one of the most important aspects is how the fingers control the force between the fingers and the handled objects. These force vectors between the fingers and the surfaces of the object describe how we interact with it, more even than the positions of the fingers themselves. Furthermore, it is these force vectors that are being accurately controlled by our neural system to optimize for grip stability and minimum intervention.

At the same time, *measuring* these forces is prohibitively difficult. Force sensors at the fingers destroy the "natural" feel and interaction, falsifying experimental data. Instrumenting objects is the obvious alternative, but leads to restricted experiments with only few objects, and restricted to predefined positions on the object.

Picking up on and extending the seminal work by Mascaro *et al.* (see, e.g., [3], [4]), we use a steady color camera to observe the nails of the fingers while in contact with an object (Fig. 1), and learn the relationship between nail coloration and force vector using convolutional neural networks (cNN) and Gaussian processes (GP). We have investigated these in two previous publications [5], [6].

Moving away from a constrained lab setting (e.g., finger brace [7]) with perfect conditions and comfortable restrictions, we focus on an additional constraint that strongly influences measurement results in this paper: the *bending* of the finger. It is easy to verify that, when you bend your finger, the color below the nail changes. The reason for this is that the extensor tendon is connected to bone underneath the nail and the tissue between nail and bone; stress there will also pull the surrounding tissue, and change the blood flow underneath the nail.

The authors are with the Faculty for Informatics, Technische Universität München, 80333 Germany nutan(at)in.tum.de, surban(at)tum.de, bayer.justin(at)gmail.com. PvdS is also with fortiss.

Fig. 1: Estimation of the finger force and torque from visual videos.

Our previous results ignored this effect, as our test settings kept the finger in approximately the same position all the time. In [8], [9] this issue is recognized and methods are proposed to estimate the angles of the finger joints from color changes. In this work, we are taking a different approach: using the (optically measured) angles of the finger joints, we use this as extra parameter for our estimator, leading to much improved accuracies when predicting the finger-exerted force from the nail image.

II. Setup

A. Experimental Apparatus

The recording setup consists of two stationary cameras and a force/torque sensor (see Fig. 2). The video data is captured by the IMAGINGSOURCE camera and ALLIED camera at 15 fps with resolutions of 1024×768 pixels and 640×480 pixels respectively. The fingernail and markers of the distal interphalangeal joint video is recorded by the IMAGINGSOURCE camera. To ensure that the markers on the back of the finger are detected for different finger joint angles, ALLIED camera is employed to record the markers of the proximal interphalangeal joint. In addition, the ATI Nano-17 six-axis force/torque sensor under the finger measures the true forces and torques of the fingertip contact point at 100 Hz. As the contact surface, a flat pad of sand paper is mounted on the sensor. We synchronize the visual and force/torque data based on time stamps. Diffuse lighting is from a white lamp. The feedback of force in the pressing direction and images are plotted on the monitor.

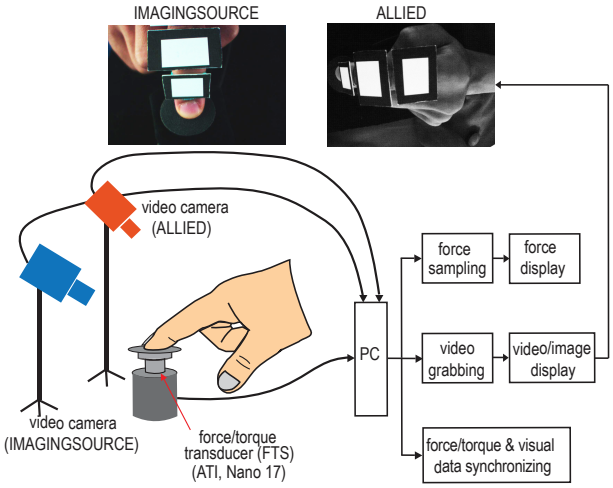

Fig. 2: Experimental apparatus. The IMAGINGSOURCE camera acquires videos of the fingertip which has contact force and toques on the ATI force/torque sensor surface. The ALLIED camera assists in finger joint angle detection.

B. Non-rigid Image Alignment

The finger orientation and location vary in the visual data. The fingernail and the surrounding skin are isolated from the finger using a color tape. After segmenting the position of the finger in the image, we continue by aligning each image to a previously recorded reference finger image; this considerably reduces subsequent processing errors. We previously demonstrated this alignment with convolutional neural networks [6] but demonstrate a different method here which has a high quality of alignment.

Nonrigid image alignment is a method that is able to locally deform the target image to fit the reference image. It plays an important role in computer vision and is widely used for a variety of applications (e.g., medical imaging and face recognition).

This method works as follows. Given a reference image I, an image J is to be aligned using non-rigid image alignment method [10]. We assume the two images have the following intensity relationship:

$$I = JT + \mathbf{v} + z \tag{1}$$

where $\mathbf{v}$ is an intensity correction field and $z \sim \mathcal{N}(0, \sigma^2)$ is zero-mean Gaussian noise. T is the geometric transformation that registers J onto I. Estimation of $\mathbf{v}$ and T is to minimize the objective function

$$E(T, \mathbf{v}) = D(I, J_v; \mathbf{v}) + w\|\mathbf{P}\mathbf{v}\|^2. \tag{2}$$

We use the sum-of-squared differences (SSD) to measure the similarity of I and J, which is given by

$$D(I, J_v; \mathbf{v}) = \sum_i \big[I(\mathbf{x}_i) - J\big(\mathbf{x}_i + \mathbf{v}(\mathbf{x}_i)\big)\big]^2. \tag{3}$$

$\|\mathbf{P}\mathbf{v}\|^2$ is a regularization term that penalizes some properties of $\mathbf{v}$. For instance, it penalizes the unsmoothness if $\mathbf{P}$ is a derivative operator. The scalar w therefore parameterizes the trade-off between the data fitness and regularization.

We model the transformation T using the free-form deformation (FFD) transformation with three hierarchical levels of B-spline control points. We update the transformation parameters via gradient descent optimization.

If images are separated into RGB channels, the fingers have a high contrast between white and red areas in the green channel, which benefits the next step of force prediction. However, the high-contrast channel creates redundant and unnecessary features, which cause misalignment during image registration, while red and blue channels are quite stable for various contact forces. Thus, the alignment transformation are generated using the blue channel of the image, and consequently, the green channel of the image is used to generate the aligned images through the transformation. Fig. 3 shows the alignment.

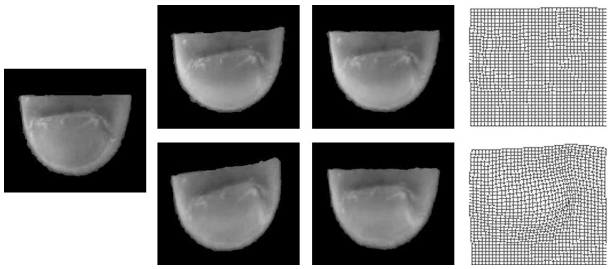

Fig. 3: Image alignment. The columns from left to right are the reference image, the images before alignment, the aligned images and the mesh transformation. The finger images are in the green channel. The more deformation of the image (row 2, column 2) has before alignment, the more mesh transformation (row 2, column 4) it is.

C. Finger Joint Estimation

Rotations in the metacarpophalangeal joint (MP, see Fig. 4) have no significant effect to the fingernail color, while rotations in the distal interphalangeal (DIP) and proximal interphalangeal (PIP) joints are relevant to the color [8]—basically, bending the finger stretches the extensor tendon and thus influences the nail bed. Thus, we focus on DIP and PIP joint angle measurements.

First of all, a rectangle marker is designed, such that the pose (position and orientation) of the rectangle can be detected by a 2D camera using HALCON (MVTec). The four line segments of the rectangle boarder are detected and the corresponding intersections are taken as corners of the rectangle. Knowing the internal camera parameters, the rectangle size in space and the detected corners, the rectangle pose in the camera space is initially estimated. After that, a non-linear optimization approach updates the final pose through minimization of the cost function, which is the geometrical distance between the detected boarders and the back projection of the space rectangle onto the image. Basically, we can compute where the rectangle is in space.

Given the coordinate of a rectangle marker, the difference in the positions of two markers can estimate a single finger

joint; we use 3 markers to estimate both DIP and PIP joint angles. For simplicity, Fig. 5 only shows PIP estimation, while DIP estimation employs the same method but with markers on distal phalanx (DP) and middle phalanx (MP). The marker sizes on MP and proximal phalanx (PP) are 1.5 cm × 2.25 cm and on DP is 1 cm × 1.5 cm. The markers on MP and PP are A and B respectively, while C is the camera coordinate.

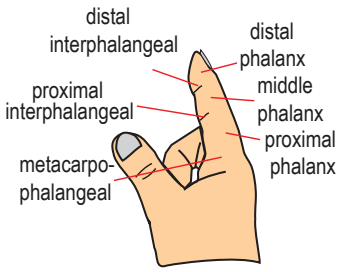

Fig. 4: Finger joint names.

$$ {}^{A}P = {}^{A}_{C}R\,{}^{C}_{B}R\,{}^{B}P = {}^{A}_{C}R\,{}^{B}_{C}R^{T}\,{}^{B}P, \tag{4} $$

where ${}^{B}P = [0, 0, 1]^T$ is a unit vector on the z direction w.r.t. the B-coordinate.

The angle of the joint is equal to angle of the 2 vectors in the z directions of the two markers.

$$ \theta_{\text{PIP}} = \text{atan2}(\|{}^{A}P \times {}^{B}P\|, {}^{A}P \cdot {}^{B}P). \tag{5} $$

The coordinates of the fingers are not strictly to be parallel in the initial positions, since we set the angle of the joint to zero in the initial position. The initial position can be at any joint angle. By default, we set the initial position when the finger is straight.

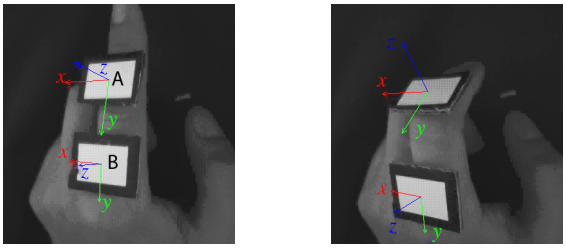

Fig. 5: Joint estimation. The left figure is the initial position of PIP. The right figure is the 38.9 degree of PIP.

III. Force/Torque Predictor

The fingernail and surrounding skin color distribution and deformation and PIP/DIP joints reflect the the changes of contact force. The force/torque predictor is to construct the mappings from the finger images and joint angles to the fingertip contact force/torque. Our method is based on Gaussian process regression to create the mappings.

One third of the consecutive data set in time is used as a test data set. The rest of the data is for training.

A. Gaussian Process Regression

A Gaussian Process (GP) [11] is one of the most widely used methods of a stochastic process. One of the essential properties is that GP is completely defined by its mean $m(\mathbf{x})$ and covariance $k(\mathbf{x}, \mathbf{x}')$ function,

$$ m(\mathbf{x}) = \mathbf{E}[f(\mathbf{x})], \tag{6} $$

$$ k(\mathbf{x}, \mathbf{x}') = \mathbf{E}\Big[\big(f(\mathbf{x}) - m(\mathbf{x})\big)\big(f(\mathbf{x}') - m(\mathbf{x}')\big)\Big]. \tag{7} $$

In a simple case without loss of generality, we assume the GP has a zero mean function. The squared exponential covariance (SE) is derived as

$$ k(\mathbf{x}, \mathbf{x}') = \sigma_f^2 \exp\Big(-\frac{1}{2l^2}\|\mathbf{x} - \mathbf{x}'\|_2^2\Big), \tag{8} $$

where the signal variance σ_f^2 and length-scale l are the hyper parameters. It is a smooth function and measures the closeness or similarity of the inputs. A basic assumption of GPs is that the target values are similar with the inputs which are close. Accordingly, the training inputs which are close to a test input have a similar target of that test input.

As the inputs of training points, $(\mathbf{x}_1, \mathbf{x}_2, \ldots, \mathbf{x_N})$ are aligned images and reshaped to 1D vectors. Additionally, the associated targets are the detected forces and torques $\mathbf{y} := (y_1, y_2, \ldots, y_N)^T$ by the force/torque sensor. Based on a training set $\{(\mathbf{x}_i, \mathbf{y}_i), i = 1, 2, \ldots, N\}$, we can obtain the predictive mean and variance of the function values f^* at test locations of the datapoints $\mathbf{x}^*$,

$$ \mathbf{E}[f^*] = \mathbf{k}^{*T}(K + \sigma_n^2 I)^{-1}\mathbf{y}, \tag{9} $$

$$ \text{Var}[f^*] = k(\mathbf{x}^*, \mathbf{x}^*) - \mathbf{k}^{*T}(K + \sigma_n^2 I)^{-1}\mathbf{k}^*, \tag{10} $$

where $K_{ij} = k(\mathbf{x_i}, \mathbf{x_j})$, $k_i^* = k(\mathbf{x_i}, \mathbf{x}^*)$, hyper parameter σ_n^2 is the noise variance, and I is denoted to identity matrix.

The optimal values for the hyper parameters $\{\sigma_f^2, l, \sigma_n^2\}$ can be evaluated from the training set by maximizing the log likelihood function

$$ \begin{aligned} \log p(\mathbf{y}|X) = &-\frac{1}{2}\mathbf{y}^T(K + \sigma_n^2 I)^{-1}\mathbf{y} \\ &-\frac{1}{2}\log\big|K + \sigma_n^2 I\big| - \frac{n}{2}\log 2\pi. \end{aligned} \tag{11} $$

B. Combined Kernel

The kernels with data coming from multiple inputs (different feature representations from subsets) can be combined. Many approaches can be chosen to combine them based on the data properties and applications. For multi-inputs of fingernail images $\mathbf{x}_{\text{im}}$ and finger joint angles $\mathbf{x}_{\text{ja}}$, we construct a kernel by the product of two kernels:

$$ \begin{aligned} k_c(\mathbf{x}, \mathbf{x}') =& k_{\text{im}}(\mathbf{x}_{\text{im}}, \mathbf{x}'_{\text{im}})k_{\text{ja}}(\mathbf{x}_{\text{ja}}, \mathbf{x}'_{\text{ja}}) \\ =& \sigma_{\text{im}}^2\sigma_{\text{ja}}^2 \exp\Big(-\frac{1}{2l_{\text{im}}^2}\|\mathbf{x}_{\text{im}} - \mathbf{x}'_{\text{im}}\|_2^2 \\ &-\frac{1}{2l_{\text{ja}}^2}\|\mathbf{x}_{\text{ja}} - \mathbf{x}'_{\text{ja}}\|_2^2\Big), \end{aligned} \tag{12} $$

where k_{im} and k_{ja} are squared exponential kernel for finger nail images and finger joint angles, respectively. The combined kernel is basically a squared exponential kernel with one length scale per modality.

The linear normalization is performed separately into the range of $[0, 1]$ for the two sources of the inputs.

C. FITC Approximation

Compared with the GP methods used in [5], the data set increases to several thousands of images and joint angles. A critical issue with GP methods is the requirement of large computation which increases as $O(N^3)$ for training, where N is the number of training samples, and $O(N^2)$ per test case. A variety of methods have been implemented to improve GPs in order to handle massive data. We choose a widely used method, fully independent training conditional approximation (FITC) (in [12] as the sparse pseudo-input GP), to accelerate the training and testing cost to $O(NM^2)$ and $O(M^2)$. The size of an inducing inputs M is much less than N. Inducing points are a small amount of inputs that summarize a large number of inputs.

To handle the large data set cases, FITC is a method that a low rank term with diagonal approximation to the exact covariance. Cross-covariance are only computed between training and inducing points as well as between test and inducing points.

We randomly select a subset of the training data as the inducing points: $\overline{\mathbf{X}} = \{\overline{\mathbf{x}}_1, \overline{\mathbf{x}}_2, ..., \overline{\mathbf{x}}_m\}$. $\mathbf{u}$ is the corresponding latent values of $\overline{\mathbf{X}}$. A more efficient likelihood approximation is given by

$$\begin{aligned} p(\mathbf{y}|\mathbf{f}) &\simeq q(\mathbf{y}|\mathbf{u}) \\ &= \mathcal{N}(K_{f,u}K_{u,u}^{-1}u, \text{diag}[K_{f,f} - Q_{f,f} + \sigma_{noise}^2 I]), \end{aligned} \tag{13}$$

where $\mathbf{f} = \{f_n\}_{n=1}^N$ are latent values based on $\mathbf{x}_n \in \mathbf{X}$, the covariance function $K_{f,f}$ is the Gram matrix all pairs $(\mathbf{x}_i, \mathbf{x}_j)$, diag[*] is a diagonal matrix of *, and $Q_{f,f} \doteq K_{f,u}$.

IV. Experiments and Results

To evaluate the implementation of the proposed approaches, experiments for the influence of joint angle and force/torque predictor are carried out. Then we will apply our methodology to measuring the forces while lifting cups with different weights.

A. Force/Torque Prediction Result

There are 5 subjects denoted by $\{S_i\}_1^5$. One finger of each subject is measured, and the subject can choose any finger. The data of the subjects are trained separately using GP and FITC-GP. The estimation is user-independently.

Without contact between the finger and the environment, DIP and PIP are dependent; in contrast, these two joints can move independently if the fingertip has a contact force [8]. In our experiments, we do not consider all permutations and combinations of the two joint angles, while the two joints are increased/decreased with the natural gestures as the finger grips objects. Additionally, as long as PIP joint degree is larger than the degree when the finger in the case of natural relaxation (θ_r), the joint degree does not influence the nail color change. Accordingly, PIP joint range is $[0, \theta_r]$ in our experiments, while other conditions can be considered as PIP at θ_r.

The subjects start from about PIP at 50 degree and DIP at 20 degree and both decrease to approximate 0 degree. For one round, the finger presses the force/torque sensor with a circle motion on the sensor surface, and at the same time increases the force slowly to about 10 N in z direction then decreases to 0. The finger is always in contact with the force/torque sensor during measurements, and the contact point is fixed. For one subject, there are 18 rounds which include 6 joint poses, about 9,000 frames and about 3,600 pixels per frame. One third of the training data are randomly selected as the inducing points for FITC.

We have the following data sets: i) data set 1, the training with the finger joint at a certain degree; ii) data set 2, the training data with the various finger joint poses; 3) data set 3, the test data with the various finger joint poses.

The results of force/torque predictor are shown in Table I (data set 2). Both of the two methods achieve high accuracy. The accuracy of FITC-GP is lower than that of GP by no more than 1% in average, but FITC-GP is considerably faster than GP. FITC-GP model is not trained using data set 1, since the result of data set 1 has low accuracy; therefore, it is meaningless to consume even more accuracy for reducing the training time. Fig. 6(a) shows an example of force and torque prediction. The figure plots only partial data for S_5, and other subjects have similar plots. The figures illustrate that the prediction matches the truth quite well and the confidence interval area is small. The R-squared accuracy ($\sqrt{R^2}$) is used to evaluate the results in quantity.

If the joint angles are relevant to the force prediction, the corresponding hyperparameters would be large. Take S_1 for instance, the combined kernel of f_z is $\{l_{ja} = 0.018, \sigma_{ja} = 0.018, l_{im} = 0.864, \sigma_{im} = -0.186\}$. Compared with about 3,600 pixels, the two joints have relative large hyperparameter values. There is an effect of the joint angle to the force prediction. In contrast, if we randomly choose any two pixels to replace the joints, the hyperparameters are $\{0.0072, 0.0072, l_{im} = 0.777, \sigma_{im} = -0.185\}$, where the first two values are l and σ of the two pixels. The two pixels have less effect to the predictor.

B. Influence of Angle Joints

Without taking the joint angle into account, the predictor may have a large error or cannot recognize the input and the result has a large confidence interval. We record two types of training data for comparison, and evaluate the effect though the same test data set. One training data set is with DIP and PIP at a certain angle and different forces. The second one contains more information with different DIP and PIP joint angles, which is described in Section IV-A. As shown in Table I, our approach strongly enhances the accuracy of the force over 10%, compared with the method ignoring the effects of various finger joints.

As an example, the comparison of our method with no joint variable in training data for S_5 is shown in Fig. 6. Specifically, the PIP angle of the test data is in the range of $[0, 40]$. The PIP joint of the training data is at 35 degree approximately for Fig. 6(b). With the difference of the joint

TABLE I: Accuracy ($\sqrt{R^2}$) of Force Estimation by Gaussian process and FITC Gaussian process. t is the training time. The measurements use the same test data set (data set 3) with different training data sets (data set 1 and data set 2). "-" means that GP cannot predict (the accuracy is negative). f and τ are force and torque respectively.

		GP (data set 2)				FITC GP (data set 2)				GP (data set 1)		
		x	y	z	t/min	x	y	z	t/min	x	y	z
S_1	f	0.952	0.959	0.966	50.7	0.949	0.958	0.963	34.0	0.728	0.823	0.863
	τ	0.951	0.966	0.956		0.951	0.962	0.955		0.807	0.440	0.667
S_2	f	0.936	0.934	0.959	49.1	0.927	0.921	0.952	37.0	0.773	0.781	0.832
	τ	0.920	0.947	0.893		0.911	0.927	0.871		0.459	-	0.459
S_3	f	0.963	0.958	0.952	52.8	0.959	0.954	0.951	30.0	0.892	0.747	0.760
	τ	0.803	0.851	0.921		0.805	0.836	0.907		0.204	0.633	0.674
S_4	f	0.962	0.961	0.961	50.7	0.963	0.961	0.957	39.7	0.891	0.801	0.659
	τ	0.934	0.891	0.900		0.931	0.871	0.899		-	-	0.544
S_5	f	0.954	0.953	0.974	31.5	0.954	0.954	0.972	25.7	0.891	0.874	0.852
	τ	0.959	0.956	0.953		0.957	0.953	0.952		0.790	0.514	0.817
$Avg.$	f	0.955	0.953	0.962	47.0	0.950	0.950	0.959	33.3	0.835	0.805	0.793
	τ	0.913	0.922	0.925		0.911	0.910	0.917		0.565	0.529	0.632

angle increasing, the error of the method without joint angle becomes larger, while the method with the various angle training data keeps the same. Especially, when PIP is at 0 degree, the fingernail always has a white area, and thus the predictor cannot predict zero f_z using data set 1.

C. Application

A task of lifting and replacing an object on a table is implemented (see Fig. 7). This application can be developed for human finger force distribution analysis for grasping and human-robot interaction. The user grip the object using thumb and forefinger. After every lifting and replacing, the fingers release and keep a distance to the object. The sensor is mounted on a container to measure the ground truth of one finger. The weight of the container and the sensor are 36 g in total, together with the standard weights increasing from 100 g to 500 g in steps of 100 g. The vertical is the sensor x direction, and the negative pressing direction is the sensor z direction. Since horizontal direction has zero force, we only plot f_x and f_z. The accuracy reaches 95.2% and 96.1% respectively.

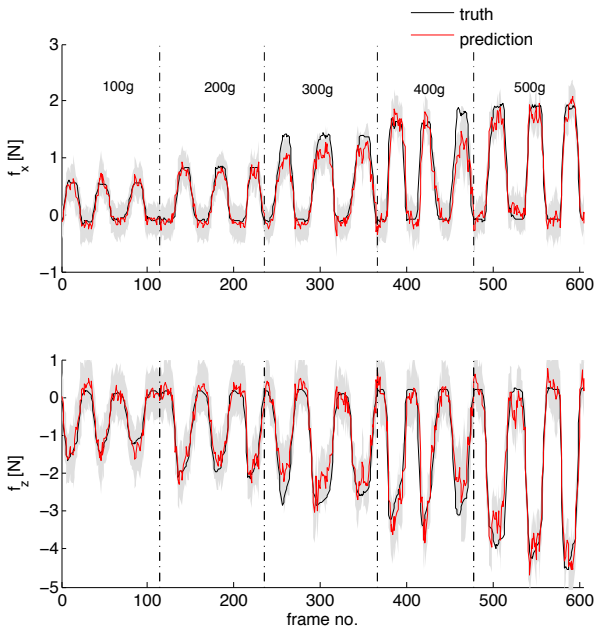

Fig. 7: Lifting and replacing objects. The gray areas are the 95% confidence interval.

V. Conclusions

This paper has presented a method that allows measuring finger contact force from the fingernail images at various finger joint angles. We compare the results of Gaussian Processes (GP) and the computationally cheaper FITC-GP with kernels combining images and visually measured joint angles. We performed experiments to quantify the estimator and present an application of lifting and replacing objects of different weight. The results demonstrate that the accuracy has been improved approximate 15% for forces and 30 % for torques with the inputs of joint angles and fingernail images. The achieved high performance enable the fingernail force estimator to strongly reduce measurement restrictions such as finger brace in real-world applications.

In the future, we will explore the approaches for multiple finger force detection, and enable the estimator to work in scenarios with more uncertainty such as different lighting conditions. Despite these restrictions, the effect of our approach is shown to be ready for applications such as human grasping and human–robot interaction.

VI. Acknowledgement

Part of this work has been supported in part by the TACMAN project, EC Grant agreement no. 610967, within the FP7 framework programme. This work has been supported in part by the Swedish Research Council, VR 2011-3128. The

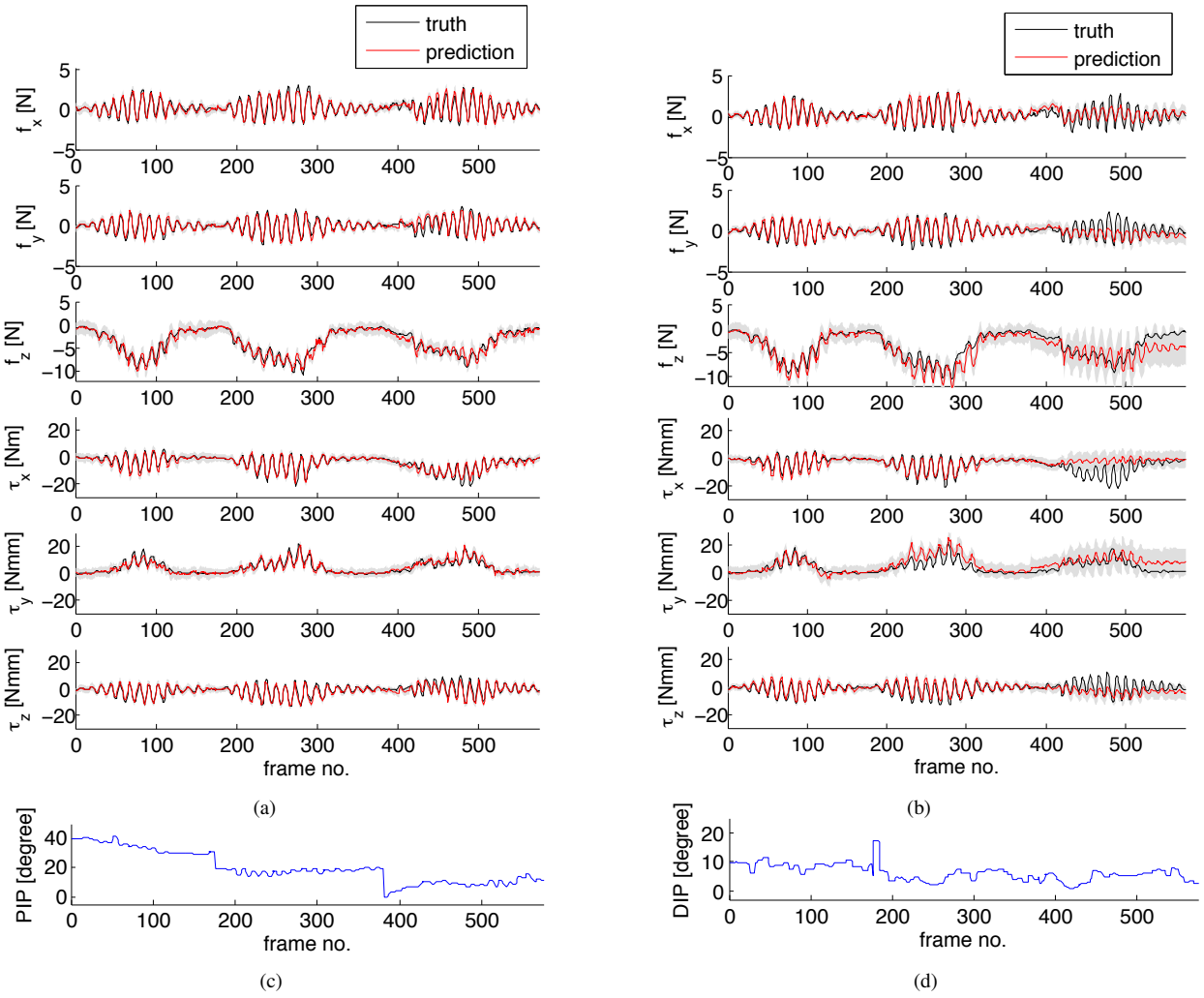

Fig. 6: Force/torque prediction for S_5. (a) shows the result of force/torque prediction using the training data set with the PIP joint angle in $[0, 50]$ degree and the DIP in $[0, 20]$ degree. (b) shows the result of force/torque prediction using the training data set with the PIP joint angle at about 35 degree. The grey areas are the 95% confidence interval. (c) and (d) are the PIP and DIP joint angles of the test data respectively. In order to increase the readability, only 3 finger joint poses are shown.

authors kindly thank Benoni Ben Edin and Göran Westling, Umeå University for their active support of this work—without them, it wouldn't have been possible.

References

[1] R. S. Johansson and J. R. Flanagan, "Sensorimotor control of manipulation," in *Encyclopedia of Neuroscience*, 8th ed., ser. Encyclopedia of Neuroscience. Elsevier, 2009, no. 8, pp. 593–604.

[2] A. Panarese and B. B. Edin, "Human ability to discriminate direction of three-dimensional force stimuli applied to the finger pad," *Journal of Neurophysiology*, vol. 105, no. 2, pp. 541–547, 2011.

[3] Y. Sun, J. Hollerbach, and S. Mascaro, "Estimation of fingertip force direction with computer vision," *IEEE Tr Robotics*, vol. 25, no. 6, pp. 1356–1369, 2009.

[4] T. Grieve, Y. Sun, J. Hollerbach, and S. Mascaro, "3-d force control on the human fingerpad using a magnetic levitation device for fingernail imaging calibration," in *EuroHaptics conference, 2009 and Symposium on Haptic Interfaces for Virtual Environment and Teleoperator Systems. World Haptics 2009. Third Joint*, 2009, pp. 411–416.

[5] S. Urban, J. Bayer, C. Osendorfer, G. Westling, B. B. Edin, and P. van der Smagt, "Computing grip force and torque from finger nail images using gaussian processes," in *IROS*, 2013.

[6] N. Chen, S. Urban, C. Osendorfer, J. Bayer, and P. van der Smagt, "Estimating finger grip force from an image of the hand using convolutional neural networks and gaussian processes," in *Proc. ICRA*, 2014.

[7] T. R. Grieve, J. M. Hollerbach, and S. A. Mascaro, "Force prediction by fingernail imaging using active appearance models," in *World Haptics Conference (WHC), 2013*, 2013, pp. 181–186.

[8] S. A. Mascaro and H. H. Asada, "Measurement of finger posture and three-axis fingertip touch force using fingernail sensors." *IEEE T. Robotics and Automation*, vol. 20, no. 1, pp. 26–35, 2004.

[9] T. Grieve, L. Lincoln, Y. Sun, J. Hollerbach, and S. Mascaro, "3d force prediction using fingernail imaging with automated calibration," in *IEEE Haptics Symposium*, 2010, pp. 113–120.

[10] A. Myronenko and X. B. Song, "Intensity-based image registration by minimizing residual complexity." *IEEE Trans. Med. Imaging*, vol. 29, no. 11, pp. 1882–1891, 2010.

[11] C. Rasmussen and C. Williams, *Gaussian Processes for Machine Learning*. MIT Press, 2006.

[12] E. Snelson and Z. Ghahramani, "Sparse gaussian processes using pseudo-inputs," in *Advances in Neural Information Processing Systems 18*. MIT Press, 2006, pp. 1257–1264.